J. Am. Soc. Mass Spectrom. (2016) 27:1165–1175
DOI: 10.1007/s13361-016-1395-z

RESEARCH ARTICLE

Difference of Electron Capture and Transfer Dissociation Mass Spectrometry on Ni^{2+}-, Cu^{2+}-, and Zn^{2+}-Polyhistidine Complexes in the Absence of Remote Protons

Daiki Asakawa,[1] Edwin De Pauw[2]

[1]National Institute of Advanced Industrial Science and Technology (AIST), Tsukuba, Ibaraki, Japan
[2]Mass Spectrometry Laboratory, Department of Chemistry, and GIGA-Research, University of Liège, B-4000, Liège (Sart-Tilman), Belgium

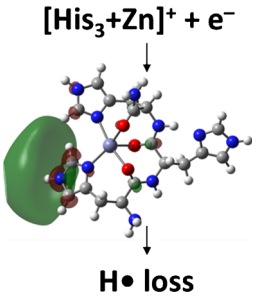

Abstract. Electron capture dissociation (ECD) and electron transfer dissociation (ETD) in metal-peptide complexes are dependent on the metal cation in the complex. The divalent transition metals Ni^{2+}, Cu^{2+}, and Zn^{2+} were used as charge carriers to produce metal-polyhistidine complexes in the absence of remote protons, since these metal cations strongly bind to neutral histidine residues in peptides. In the case of the ECD and ETD of Cu^{2+}-polyhistidine complexes, the metal cation in the complex was reduced and the recombination energy was redistributed throughout the peptide to lead a zwitterionic peptide form having a protonated histidine residue and a deprotonated amide nitrogen. The zwitterion then underwent peptide bond cleavage, producing *a* and *b* fragment ions. In contrast, ECD and ETD induced different fragmentation processes in Zn^{2+}-polyhistidine complexes. Although the N–C_α bond in the Zn^{2+}-polyhistidine complex was cleaved by ETD, ECD of Zn^{2+}-polyhistidine induced peptide bond cleavage accompanied with hydrogen atom release. The different fragmentation modes by ECD and ETD originated from the different electronic states of the charge-reduced complexes resulting from these processes. The details of the fragmentation processes were investigated by density functional theory.

Keywords: Metal reduction, Zwitterion formation, Hydrogen radical loss, Peptide bond cleavage, Density functional theory calculation

Received: 8 February 2016/Revised: 18 March 2016/Accepted: 22 March 2016/Published Online: 20 April 2016

Introduction

Electrospray ionization (ESI)-based tandem mass spectrometry with electron-mediated fragmentation techniques, such as electron capture dissociation (ECD) [1] and electron transfer dissociation (ETD) [2], have been widely used for peptide/protein sequencing [3–5]. ECD/ETD is initiated by electron attachment/transfer to multiply-protonated molecules, which induces cleavage at N–C_α bonds in the peptide backbone. Several ECD/ETD mechanisms have been investigated in order to understand this phenomenon [6–11]. In one such mechanism, the so-called Cornell model, the recombination of an electron and an excess proton in a multiply protonated molecule, followed by the transfer of the resulting hydrogen atom to a carbonyl group in the peptide backbone, eventually forms a $c'/z^\bullet$ fragment pair [6]. Alternatively, in the Utah-Washington model, direct electron attachment to the π* amide orbital of the backbone amide group produces c'- and $z^\bullet$-radical fragments via a fragile aminoketyl radical-anion intermediate [8, 9]. This intermediate can undergo N–C_α bond cleavage to form iminoenol c' anion and $z^\bullet$ fragments. The anion charge in the c' fragment is then neutralized by proton transfer, forming an amide c' fragment.

In a previous study by Asakawa, et al. [12], Zn^{2+}-polyhistidine complexes in the absence of remote protons were used in order to elucidate whether the process proceeded via the Cornell or the Utah-Washington model. Electron transfer to the Zn^{2+}-polyhistidine complex from a fluoranthene radical anion produced a zwitterionic zinc-peptide radical. Subsequently, the donation of an electron from the N–C_α bond to the nitrogen

Electronic supplementary material The online version of this article (doi:10.1007/s13361-016-1395-z) contains supplementary material, which is available to authorized users.

Correspondence to: Daiki Asakawa; *e-mail:* d.asakawa@aist.go.jp

atom produced $[Zn/c'–H/z•]^{+•}$ complex consisting of the iminoenol *c'* anion and a $z^{•}$ radical having a radical site on the α-carbon atom. Presumably, the intermediate complex can undergo multistep interfragment proton transfer reactions, which stabilize the resulting fragments. Finally, $[z_n•–H + Zn]^{+•}$ and $[c'_n–H + Zn]^{+}$ were generated by ETD. This combined experimental and computational study provided clear evidence for the validity of the Utah-Washington model for ETD.

In the case of a protonated precursor, metal-peptide complexes give a *c'*/*z•* fragment pair by ECD/ETD for most metal cations [13–19], suggesting that the fragmentation proceed via Utah-Washington model. In contrast, transition metal cations with a partially filled *d* orbital shell, such as Co^{2+}, Ni^{2+}, and Cu^{2+}, are reduced by ECD/ETD [15, 20]. In that case, the fragmentation is mainly induced by the substantial excitation attributable to the energy of the recombination of the metal cation in the complex and the electron, instead of radical-induced N–$C_α$ bond cleavage. Tureček et al. investigated the ECD/ETD process of complexes containing a peptide and a transition metal by density functional theory (DFT) calculation [21–23]. They found that the fragmentation process was dependent on the metal cation in the complex, indicating that the properties of the metal cation dictated the ECD/ETD process.

In the case of transition metal cations with a partially filled *d* orbital shell, the presence of a protonated histidine residue also suppresses N–$C_α$ bond cleavage during ECD and ETD [24, 25]. Electron attachment to the protonated histidine residue produces an imidazoline radical of the [1H,3H]-type, which undergoes an exothermic hydrogen radical rearrangement to form an isomeric radical having a [1H,2H]-type imidazoline group [24]. In the ETD mass spectrum, the intact electron-transfer product produces an intense signal owing to the high stability of the [1H,2H]-type imidazoline radical [25–27]. In contrast to ETD, ECD of a protonated histidine-containing peptide induces loss of a hydrogen radical via a [1H,2H]-type imidazoline radical, followed by the backbone dissociation of even-electron ions [28].

In the present study, we employ Ni^{2+}, Cu^{2+}, and Zn^{2+} as charge carriers to produce metal-polyhistidine complexes in the absence of remote protons, since these cations strongly bind to the neutral histidine residues of peptides or proteins. The absence of remote protons in the precursor ions facilitates the investigation of the fragmentation pathway by DFT calculation. ECD and ETD of the Ni^{2+}- and Cu^{2+}-polyhistidine complexes produce fragment ions via peptide bond cleavage. As previously reported, ETD of the Zn^{2+}-polyhistidine leads to N–$C_α$ bond cleavage via aminoketyl anion radical formation [12]. In contrast, ECD of this complex induces peptide bond cleavage accompanied with hydrogen atom loss. The details of the ETD and ECD processes are investigated.

Experimental

Materials and Preparation

Amidated L-histidine oligomers (HHH-NH_2, HHHH-NH_2, and HHHHH-NH_2) were purchased from Medical and Biological Laboratories Co., Ltd. (Nagoya, Japan). Cupper chloride ($CuCl_2$), zinc chloride ($ZnCl_2$), nickel chloride ($NiCl_2$), and acetic anhydride were purchased from Wako Pure Chemical (Osaka, Japan). All reagents were used without further purification. All the solvents used were HPLC grade quality, except for water, which was purified by Milli-Q purification system (Millipore; Billerica, MA, USA). Analyte peptides were acetylated by 1% acetic anhydride aqueous solution at room temperature for 1 h and then the excess reagent and solvent were removed by centrifugal evaporator.

Mass Spectrometry

The analyte peptides were dissolved in water/methanol (1/1, v/v) at a concentration of 10 μM. To produce metal-peptide complex, metal chloride was added to the peptide solution at 100 μM. The ETD and ECD MS/MS experiments were performed using a quadrupole ion trap mass spectrometer (AmaZon X; Bruker, Germany) and a 9.6 T FT-ICR mass spectrometer (SolariX FT; Bruker, Germany), respectively. The analyte solution directly infused into the mass spectrometer using ESI ion source. For ETD fragmentation, fluoranthene radical anion was used for reaction and the ion/ion reaction time was set at 250 ms. For ECD experiment, precursor ions were mass-selected in the quadrupole filter and then transmitted to ICR cell. The peptide ions were fragmented by ECD in the cell. The cathode dispenser was heated gradually to 1.7 A prior to performing experiments. The ECD pulse length was set at 7 ms, and the ECD bias was 0.7 V.

Calculations

All electron structure calculations were performed with Gaussian 09 program [29]. The geometries for zinc-trihistidine complexes were optimized with DFT calculations using the M06-2X [30] hybrid functional and 6-31+G(d,p) basis set on C, H, O, N and outer shell electron of transition metals, Ni, Cu, and Zn. The core electrons in the Cu and Zn were handled by the LanL2DZ effective core potential (ECP). The obtained geometries were characterized by frequency calculations as local energy minima and the harmonic frequencies were used to obtain zero-point energy corrections. To establish the energetics for fragmentation, transition state geometries were also optimized at the M06-2X/ECP/6-31+G(d,p) level and investigated by examining their vibrational frequency analysis, showing one imaginary frequency. The relationship between transition state and the reactants, as well as intermediates, was checked by an intrinsic reaction coordinate analysis [31] starting from the transition state conformation. Single-point energies of local energy minima and transition state geometries were calculated using M06-2X functions with 6-311++G(2d,p) basis set. Excited electronic states were calculated using time-dependent DFT method [32] with the M06-2X functional and the 6-311++G(2d,p) basis set.

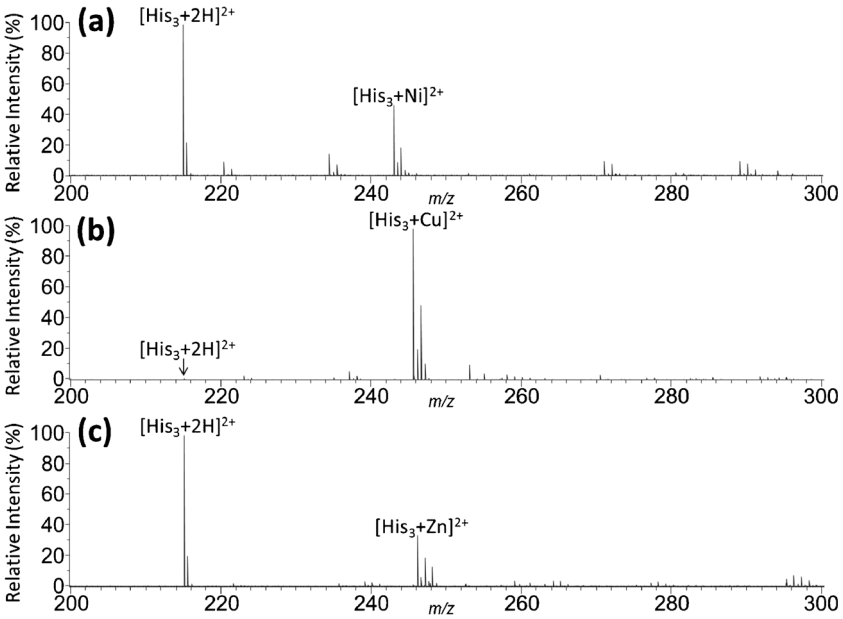

Figure 1. ESI mass spectra of 10 μM His_3 with (**a**) 100 μM $NiCl_2$, (**b**) 100 μM $CuCl_2$, and (**c**) 100 μM $ZnCl_2$ recorded by FT-ICR mass spectrometer

Notation

In the present study, Zubarev's unambiguous notation was adopted for peptide fragment ions [33]. According to this notation, homolytic N–C_α bond cleavage yields the radical *c*• and *z*• fragments, and addition of a hydrogen atom to *c*• or *z*• fragments produces *c′* or *z′* fragment, respectively. The abstraction of a hydrogen atom from *c*• or *z*• fragments produces *c* or *z* fragment, respectively. The example of the notation is shown in Supplemental Information, Scheme S1.

Results and Discussion

ETD of Ni^{2+}-, Cu^{2+}-, and Zn^{2+}-Trihistidine

The Ni^{2+}-, Cu^{2+}-, and Zn^{2+}-trihistidine complexes were used as model systems to investigate the mechanisms of ETD and ECD fragmentation. As in the case of the first author's previous study, we focused on the involvement of remote protons, and the C-terminal carboxyl group in the trihistidine was amidated to avoid the production of remote protons in the complex. The

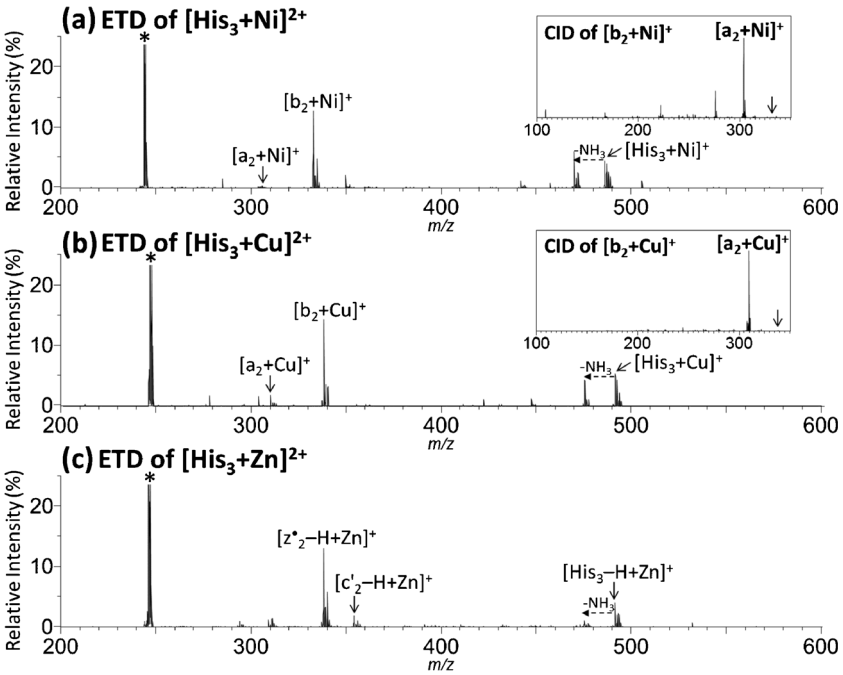

Figure 2. ETD mass spectra of metal- trihistidine complexes, (**a**) $[His_3 + Ni]^{2+}$, (**b**) $[His_3 + Cu]^{2+}$, and (**c**) $[His_3 + Zn]^{2+}$. Inset panel: CID MS^3 mass spectra of $[a_2 + Ni]^+$ and $[a_2 + Cu]^+$

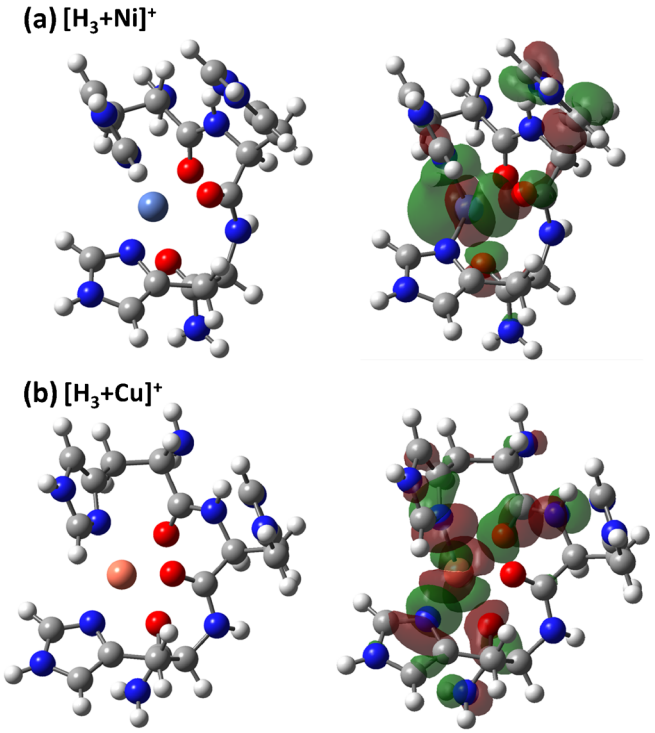

Figure 3. Structure and highest occupied molecular orbital (HOMO) of the charge-reduced metal-peptide complexes, (**a**) $[His_3 + Ni]^{+\bullet}$ and (**b**) $[His_3 + Cu]^+$. The molecular orbitals were obtained by single-point energy calculations with the M06-2X/6-311++G(2d,p) basis set on M06-2X/ECP/6-31+G(d,p)-optimized geometries

ESI mass spectra of amidated trihistidine (His_3) with 100 μM transition metal chlorides ($NiCl_2$, $CuCl_2$, and $ZnCl_2$) were compared, as shown in Figure 1. The results indicate that the order of the metal-peptide complex yield is $Cu^{2+} > Ni^{2+} \geq Zn^{2+}$, which corresponds to the increasing binding energy between the divalent metal cation and the imidazole group in histidine residues. In particular, the Cu^{2+}-aided method produces an intense signal for the Cu^{2+}-His_3 complex at *m/z* 245.6, instead of $[His_3 + 2H]^{2+}$ at *m/z* 215.1, due to the strong interaction between Cu^{2+} and the neutral imidazole group in the histidine residues.

Subsequently, we used the doubly charged complexes $[His_3 + Ni]^{2+}$, $[His_3 + Cu]^{2+}$, and $[His_3 + Zn]^{2+}$ as precursor ions for ETD MS^2 measurement in an ion trap mass spectrometer. The ETD mass spectra of these ions are shown in Figure 2. The details of the ETD fragmentation of $[His_3 + Zn]^{2+}$ have been described in a previous report by the first author [12]. In brief, electron transfer to $[His_3 + Zn]^{2+}$ produces an aminoketyl radical-anion intermediate, which immediately undergoes N–C_α bond cleavage. In contrast to $[His_3 + Zn]^{2+}$ (Figure 2c), ETD of $[His_3 + Ni]^{2+}$ and $[His_3 + Cu]^{2+}$ generate the singly charged metal adduct b_2 fragment, indicating that the metal cations in the products are the monovalent form, i.e., Ni^+ and Cu^+ (Figure 2a and b). The Ni^{2+} and Cu^{2+} in the complexes are reduced by ETD, and the energy from the recombination of the metal cation and fluoranthene radical anion is redistributed throughout the peptide to give b_2 fragments. Additionally, $[a_2 + Ni]^+$ and $[a_2 + Cu]^+$ are observed as weak signals in the ETD mass spectra of $[His_3 + Ni]^{2+}$ and $[His_3 + Cu]^{2+}$, respectively. The activation of protonated *b* ions often produces *a* ions by loss of carbon monoxide [34]. In order to confirm the generation of $[a_2 + metal]^+$ from $[b_2 + metal]^+$, we performed MS^3 analysis with collision-induced dissociation (CID). As shown in the insets of Figure 2a and b, CID of $[b_2 + metal]^+$ selectively leads to $[a_2 + metal]^+$, suggesting that the $[a_2 + Ni]^+$ and $[a_2 + Cu]^+$ signals in the ETD spectra are generated by decomposition of $[b_2 + Ni]^+$ and $[b_2 + Cu]^+$, respectively.

Fragmentation Mechanism of the Cu^{2+}-Trihistidine Complex by DFT Calculation

The details of the ETD of $[His_3 + Ni]^+$ and $[His_3 + Cu]^+$ were investigated by DFT calculation. In order to discuss the initial step of ETD in $[His_3 + Ni]^{2+}$ and $[His_3 + Cu]^{2+}$, we calculated the electron structures of the precursor ions and their charge-reduced products. The energy minimization in gas phase

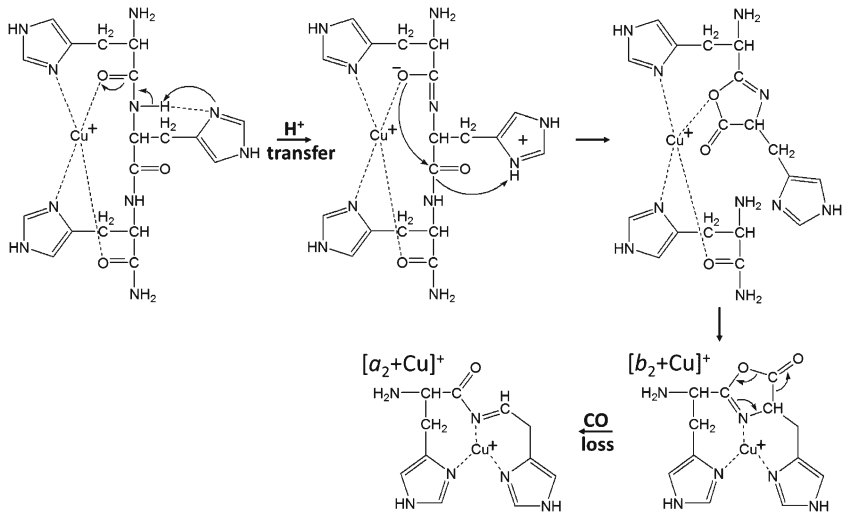

Scheme 1. Potential fragmentation pathway of $[His_3 + Cu]^{2+}$ by ETD and CID

usually occurs through intramolecular charge solvation. In the stable conformations of metal-His_3 complexes, metal cation was coordinated by the side chains of His^1 and His^3, and backbone carbonyl oxygens. The lowest-energy conformations of $[His_3 + Ni]^+$ and $[His_3 + Cu]^+$ are shown in Figure 3. An electron in the highest occupied molecular orbital (HOMO) of $[His_3 + Ni]^+$ and $[His_3 + Cu]^+$ is present in the $d_{(x^2-y^2)}$ and d_z^2-orbital of Ni^+ and Cu^+, respectively, indicating that the metal cations in $[His_3 + Ni]^{2+}$ and $[His_3 + Cu]^{2+}$ are reduced by ETD. As shown in Figure 2, ETD of $[His_3 + Ni]^{2+}$ and $[His_3 + Cu]^{2+}$ gave $[a_2 + metal]^+$, $[b_2 + metal]^+$, and $[His_3–NH_3 + metal]^+$. The presence of Cu^{2+} instead of Ni^{2+} in the precursor does not significantly influence the yield of fragment ions. These experimental and theoretical results suggest that the ETD of $[His_3 + Ni]^{2+}$ and $[His_3 + Cu]^{2+}$ shares some mechanistic similarities each other (i.e., ETD induces metal reduction with subsequent fragmentation driven by recombination energy). In order to investigate the fragmentation of metal-peptide complexes induced by metal reduction, we focused on the formation mechanisms of $[b_2 + Cu]^+$ and $[a_2 + Cu]^+$ by DFT calculation, since the calculation of electron structure of Cu^+ (even-electron) is easier than that of Ni^+ (odd-electron).

As described above, electron transfer to $[His_3 + Cu]^{2+}$ induces peptide bond cleavage, and the resultant $[b_2 + Cu]^+$ undergoes carbon monoxide loss by CID. The potential fragmentation pathway of $[His_3 + Cu]^{2+}$ by ETD and CID is shown in Scheme 1. First, we focused on the formation mechanism of $[b_2 + Cu]^+$. In the case of protonated peptides, their activation leads to the formation of various species containing different protonation sites by relocation of the excess protons. Since the peptide bond is weakened by the protonation of the backbone amide nitrogen, formation of *b* and *y*' ions is often mediated by a mobile proton [35]. Recently, the protonated histidine residue has been reported to mediate peptide bond cleavage by proton mobilization [36]. Consequently, the mechanism of peptide

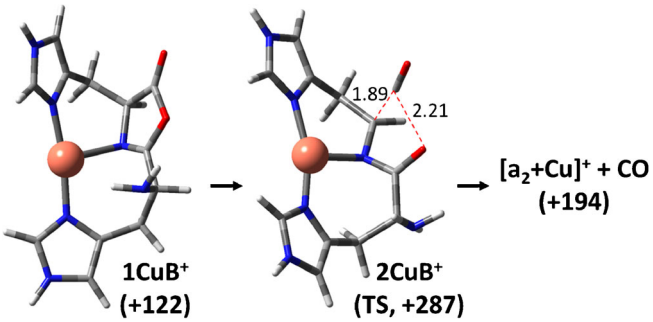

Scheme 3. Formation mechanism of $[a_2 + Cu]^+$ fragment from $[b_2 + Cu]^+$ by carbon monoxide loss. The relative energy (kJ/mol) were obtained by single-point energy calculations with the M06-2X/6-311++G(2d,p) basis set on M06-2X/ECP/6-31+G(d,p)-optimized geometries including M06-2X/ECP/6-31+G(d,p) zero-point vibrational energies

bond cleavage in the charge-reduced $[His_3 + Cu]^+$ complex was considered in terms of proton mobilization, even though the $[His_3 + Cu]^+$ complex does not contain any remote protons.

The energy from the recombination of a complex and an anion generates a zwitterionic product in which the amide nitrogen is deprotonated and a proton is present on the histidine residue. Proton transfer between the amide nitrogen of His^1 and the imidazole group of His^2 in $1Cu^+$ proceeds through transition state $2Cu^+$, which is 116 kJ/mol above $1Cu^+$, resulting in the zwitterionic complex, $3Cu^+$. The proton present on the imidazole group is then transferred to the amide nitrogen on the His^3 residue. The corresponding transition state $4Cu^+$ is 77 kJ/mol above $3Cu^+$. The resultant complex $5Cu^+$ has a labile peptide bond, and the transition state barrier for the peptide bond cleavage is only 8 kJ/mol. Consequently, $5Cu^+$ immediately undergoes peptide bond cleavage, resulting in the formation of the complex $7Cu^+$, in which the oxazolone b_2 and y'_1 are linked together via the Cu^+ ion that coordinates with the

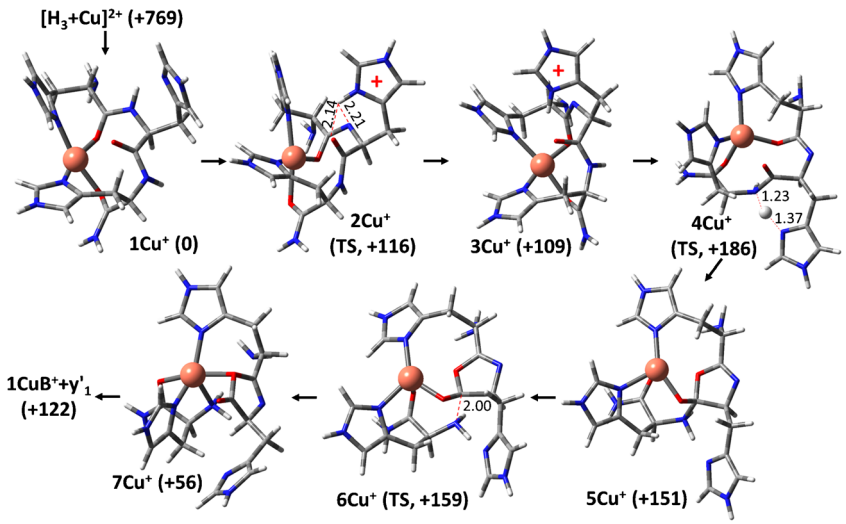

Scheme 2. Formation mechanism of $[b_2 + Cu]^+/y'_1$ fragment pair from $[His_3 + Cu]^+$. The relative energy (kJ/mol) were obtained by single-point energy calculations with the M06-2X/6-311++G(2d,p) basis set on M06-2X/ECP/6-31+G(d,p)-optimized geometries including M06-2X/ECP/6-31+G(d,p) zero-point vibrational energies

Table 1. Energies of Transition State Barrier of ECD/ETD Fragmentation on $[His_3 + Cu]^{2+}$ Obtained from Single-Point Energy Calculations with the M06-2X/6-31++G(2d,p) Basis Set on M06-2X/ECP/6-31G(d) Optimized Geometries Including M06-2X/ECP/6-31G(d) Zero-Point Vibrational Energies (kJ/mol)

$1Cu^+ \rightarrow 2Cu^+$	$3Cu^+ \rightarrow 4Cu^+$	$5Cu^+ \rightarrow 6Cu^+$	$1CuB^+ \rightarrow 2CuB^+$
116	77	8	165

imidazole groups, amino group, and carbonyl oxygen atoms. The products, Cu^+-adducted oxazolone b_2 and y'_1 are less stable than $1Cu^+$ by 122 kJ/mol. The dissociation processes leading to $[b_2 + Cu]^+$ and y'_1 are summarized in Scheme 2.

Next, the mechanism of $[a_2 + Cu]^+$ formation from $[b_2 + Cu]^+$ was investigated. In the optimized conformation of $[b_2 + Cu]^+$ ($1CuB^+$), b_2 and Cu^+ are coordinated through the imidazole groups and the nitrogen atom in the oxazolone group. Carbon monoxide loss proceeds through transition state $2CuB^+$, which is 165 kJ/mol above $1CuB^+$. Finally, the formation energy of $[a_2 + Cu]^+$ and carbon monoxide is 72 kJ/mol above $1CuB^+$. These dissociation processes are summarized in Scheme 3. The transition state barriers for the fragmentation of $[His_3 + Cu]^+$ are summarized in Table 1.

ECD of Cu^{2+}-Polyhistidine Complexes

The ECD of $[His_3 + Cu]^{2+}$ was also investigated (Figure 4). Compared with the ETD, the ECD of $[His_3 + Cu]^{2+}$ is more prone to $[a_2 + Cu]^+$ formation than $[b_2 + Cu]^+$ formation. The major differences between ECD and ETD are the recombination process and pressure during fragmentation. Capture of a free electron by an ion in the gas phase can be characterized by the ion adiabatic recombination energy, and ECD in the FTICR mass spectrometer occurs without collision with background gas. Consequently, the internal energy of the charge-reduced complex generated by ECD would be in the 500–800 kJ/mol range. In contrast, the internal energies of the ETD products can be estimated from the energy balance between the ion adiabatic recombination energy, the electron affinity of fluoranthene, and the excitation energy in the neutral fluoranthene molecule. For ETD experiments, the ion trap is operated using a collision gas, and therefore the internal energy of the ETD products are decreased by collision with the gas. As a result, the electron-transfer reaction between the peptide dication and the fluoranthene anion generates a peptide radical cation with 285–327 kJ/mol of vibrational excitation [37]. Compared with ETD, the high abundance of $[a_2 + Cu]^+$ in the ECD mass spectrum can be understood by considering the high vibrational excitation of $[b_2 + Cu]^+$.

Next, to investigate the effect of the peptide size in the complex on the ECD process, trihistidine with N-terminal acetylation and C-terminal amidation ($AcHis_3$) and *N*-acetyl-C-amide-tetrahistidine ($AcHis_4$) were used for comparison (Figure 4). As in the case of the ECD of $[His_3 + Cu]^{2+}$, the formation of $[b_n + Cu]^+$ and $[a_n + Cu]^+$ is induced by the ECD of $[AcHis_3 + Cu]^{2+}$ and $[AcHis_4 + Cu]^{2+}$. Notably, the yield of $[a_n + Cu]^+$ is dependent on the peptide size. The order of the $[a_n + Cu]^+$ yield is $[His_3 + Cu]^{2+} > [AcHis_3 + Cu]^{2+} > [AcHis_4 + Cu]^{2+}$, which corresponds to an increase the complex size. As described above, the $[a_n + Cu]^+$ would be generated by further degradation of $[b_n + Cu]^+$. When the number of vibrational modes increases, the yield of $[a_n + Cu]^+$ decreases because there is less energy received per mode. Moreover, the recombination energy of the complexes and transition state barrier for the fragmentation would change with complex size, since a larger complex is more able to accommodate the extra

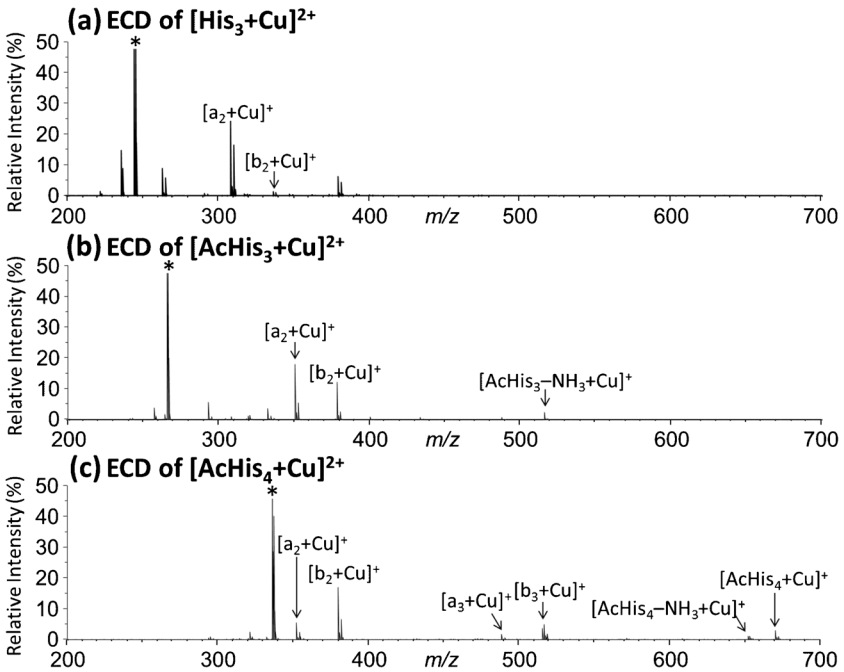

Figure 4. ECD mass spectra of Cu^{2+}- trihistidine complexes, (**a**) $[His_3 + Cu]^{2+}$, (**b**) $[AcHis_3 + Cu]^{2+}$, and (**c**) $[AcHis_4 + Cu]^{2+}$

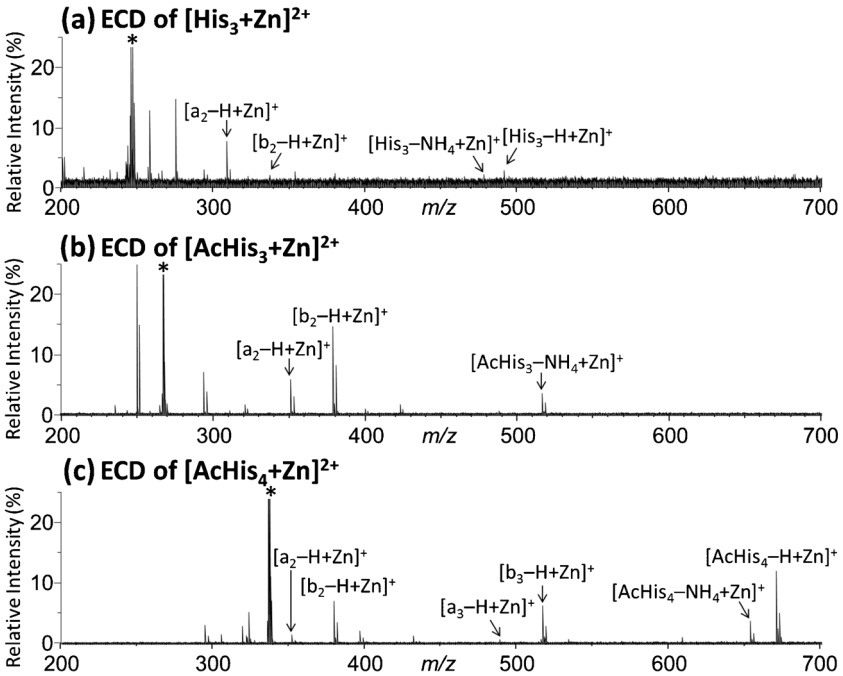

Figure 5. ECD mass spectra of Zn^{2+}-trihistidine complexes, (**a**) $[His_3 + Zn]^{2+}$, (**b**) $[AcHis_3 + Zn]^{2+}$, and (**c**) $[AcHis_4+Zn]^{2+}$

electron. The effect of the peptide size in the complex on the ETD process is also investigated as well as ECD. ETD mass spectra of $[AcHis_3 + Cu]^{2+}$, $[AcHis_4 + Cu]^{2+}$, and $[AcHis_5+Cu]^{2+}$ are shown in Supplemental Information, Figure S1. In summary, the increasing of peptide size in the complex suppresses the fragmentation.

ECD of Zn^{2+}-Polyhistidine Complexes

Next, we investigated the ECD of Zn^{2+}-polyhistidine complexes (Figure 5), which differs dramatically from the ETD (Figure 2c). Although ETD of Zn^{2+}-polyhistidine complexes gives fragment ions due to N–C_α bond cleavage [12], the $[z^{\bullet}{}_n–H + Zn]^+$ and $[c'_n–H + Zn]^+$ fragments are not observed in the ECD spectra. Conversely, signals due to $[b_2–H + Zn]^+$ and $[a_2–H + Zn]^+$ are observed. As in the case of ECD of $[His_n + Cu]^{2+}$ (Figure 4), the yield of metal-adducted a_n ions from $[His_n + Zn]^{2+}$ decreases with the size of complexes (Figure 5). The experimental results suggest that ECD of Zn^{2+}-polyhistidine complexes produced [1H,2H]-type imidazoline radical, instead of aminoketyl radical anion intermediate. As described in the Introduction section, the formation of [1H,2H]-

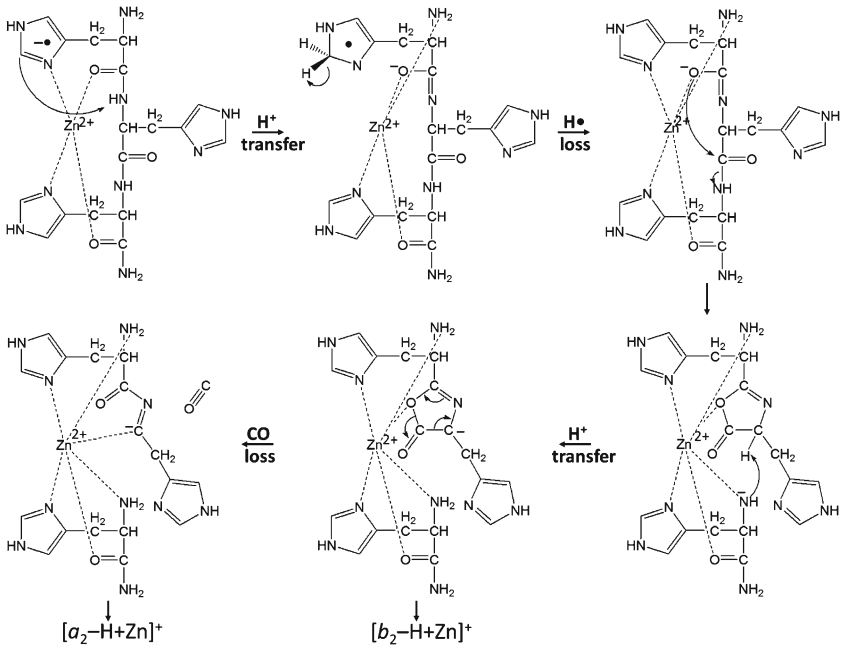

Scheme 4. Potential fragmentation pathway of $[His_3 + Zn]^{2+}$ by ECD

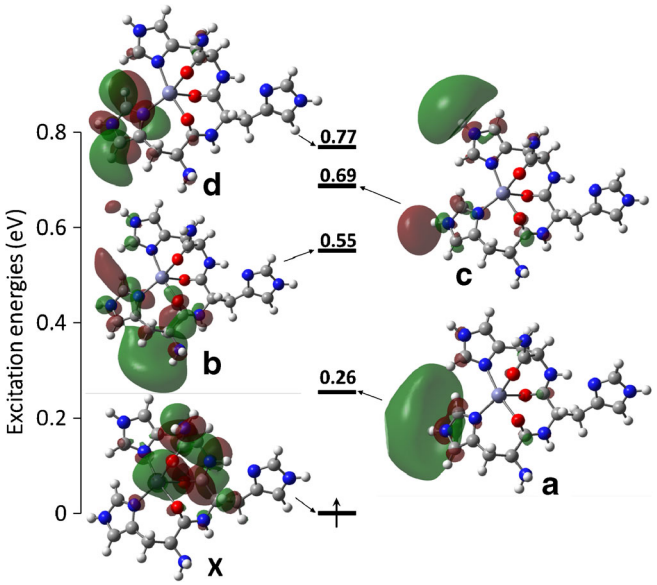

Figure 6. Electronic state diagram for vertical electron attachment to $[His_3 + Zn]^{2+}$. The excitation energies (eV) are from TD-M06-2X/6-311++G(2d,p) calculations

type imidazoline radical suppress the radical-induced N–C_α bond cleavage because of that high stability. Herein, the formation processes of $[b_n–H + Zn]^+$ and $[a_n–H + Zn]^+$ is considered in terms of ECD-induced hydrogen radical loss followed by fragmentation of the even-electron complex $[His_n–H + Zn]^+$. The potential fragmentation pathway of $[His_3 + Zn]^{2+}$ by ECD are shown in Scheme 4 and the detail of the fragmentation processes were investigated by DFT calculation.

ECD Fragmentation Mechanism of Zn^{2+}-Trihistidine Complexes by DFT Calculation

The dramatic differences in the fragmentation of $[His_3 + Zn]^{2+}$ induced by ECD and ETD originate from the different electronic states of the charge-reduced complexes formed by these different processes. Consequently, we first discussed the electronic states of charge-reduced complexes. Figure 6 shows the molecular orbitals for the first four excited electronic states of the charge-reduced Zn^{2+}-His_3 complex and their corresponding vertical excitation energies. As discussed in our previous report, the ground state of the charge-reduced complex, X in Figure 6, immediately undergoes N–C_α bond cleavage via a zwitterionic aminoketyl radical intermediate [12]. In contrast, the charge-reduced product formed from excited state configurations undergoes hydrogen radical transfer, giving a long-lived radical intermediate with a [1H,2H]-type imidazoline group, as in the case of protonated molecules. The N–C_α bond cleavage is suppressed by the presence of a [1H,2H]-type imidazoline group due to its high stability. Instead of radical-induced dissociation, the [1H,2H]-type imidazoline group is reported to release a hydrogen radical [27, 28]. The processes of the [1H,2H]-type imidazoline group formation and subsequent hydrogen loss are summarized in Scheme 5. The hydrogen transfer from backbone amide to C-2 position in the imidazole at His1 residue produced [1H,2H]-type imidazoline group through transition state $2Zn^+$•, which is 196 kJ/mol above $1Zn^+$•. Subsequently, the resulted $3Zn^+$• undergoes the loss of a hydrogen radical from the C-2 position in the [1H,2H]-type imidazoline group. The corresponding transition state, $4Zn^+$•, is 132 kJ/mol above $1Zn^+$•, producing the even-

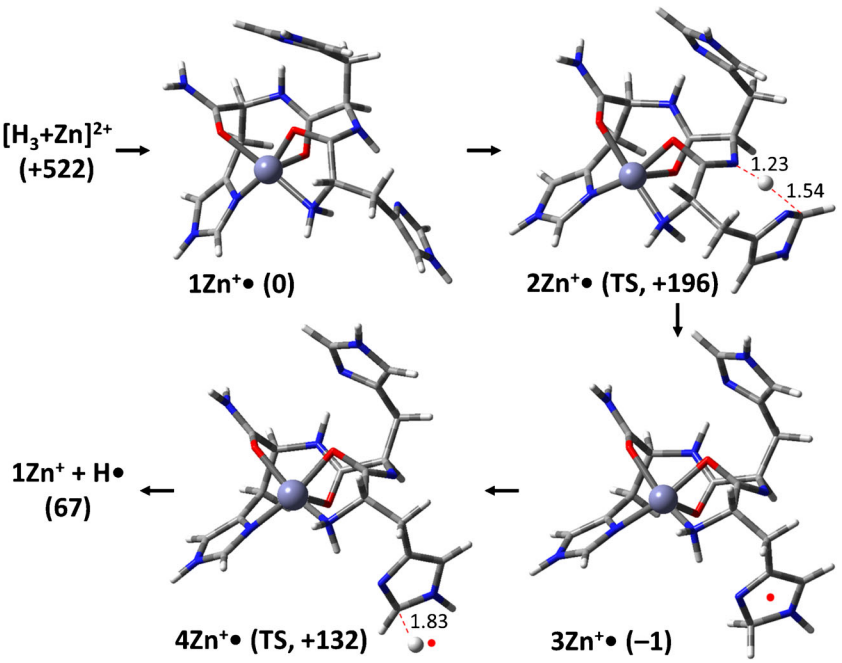

Scheme 5. The processes of hydrogen loss from $[His_3 + Zn]^+$•. The relative energy (kJ/mol) were obtained by single-point energy calculations with the M06-2X/6-311++G(2d,p) basis set on M06-2X/ECP/6-31+G(d,p)-optimized geometries including M06-2X/ECP/6-31+G(d,p) zero-point vibrational energies

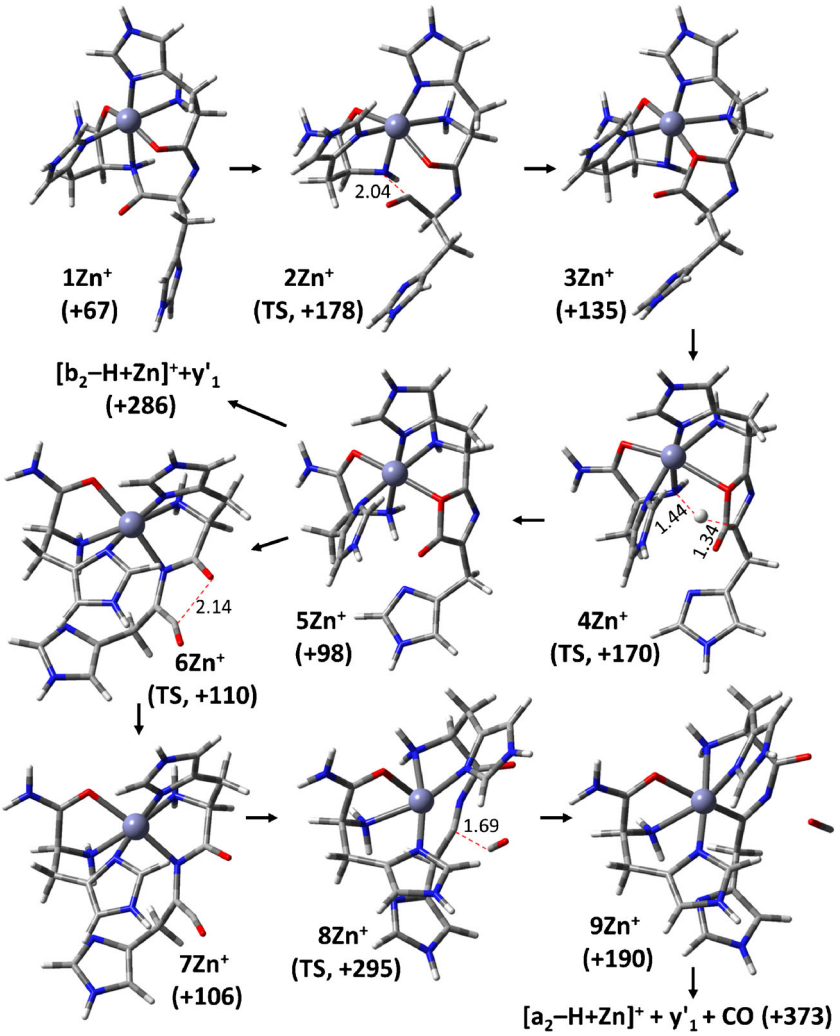

Scheme 6. Formation mechanism of $[b_2 - H + Zn]^+$ fragment from $[His_3(NH_2) - H + Zn]^+$. The relative energy (kJ/mol) were obtained by single-point energy calculations with the M06-2X/6-311++G(2d,p) basis set on M06-2X/ECP/6-31+G(d,p)-optimized geometries including M06-2X/ECP/6-31+G(d,p) zero-point vibrational energies

electron complex $1Zn^+$ and a free hydrogen radical. The formation energy of $1Zn^+$ and a hydrogen atom is 67 kJ/mol above $1Zn^+$•.

Next, we considered the formation processes of $[b_2–H + Zn]^+$ by peptide bond cleavage of the even-electron complex $1Zn^+$ containing a deprotonated amide group (Scheme 6). In the case of CID of the deprotonated peptide, the negative charge on the amide group is reported to induce peptide bond cleavage, forming oxazolone *b* and deprotonated *y*' fragments [38]. Although the intermediate $1Zn^+$ is a singly charged positive ion, the negative charge on amide nitrogen would induce peptide bond cleavage, producing oxazolone *b* and deprotonated *y*' fragments. The peptide bond cleavage of $1Zn^+$ was calculated to proceed via transition state $2Zn^+$, which is 111 kJ/mol above $1Zn^+$, and the complex $[Zn/b_2/y'_1–H]^+$ ($3Zn^+$) is formed. Since the final product on ECD of $[His_3 + Zn]^{2+}$ was $[b_2–H + Zn]^+$, the $[y'_1–H]^-$ in $3Zn^+$ abstracts a proton from the oxazolone b_2 ring α-carbon atom. The corresponding transition state for interfragment proton transfer is $4Zn^+$, which is 35 kJ/mol above $3Zn^+$, and the resultant complex $5Zn^+$ is more stable than $3Zn^+$ by 37 kJ/mol. Finally, the formation of $[b_2–H + Zn]^+$ and y'_1 from $1Zn^+$• requires 286 kJ/mol.

In contrast to $[b_2–H + Zn]^+$ formation, the deprotonated oxazolone b_2 fragment in $5Zn^+$ give $[a_2–H + Zn]^+$, y'_1, and carbon monoxide by further degradation. The formation of $[a_2–H + Zn]^+$ from $[b_2–H + Zn]^+$ is also described in

Table 2. Energies of Transition State Barrier of ECD Fragmentation on $[His_3 + Zn]^{2+}$ Obtained From Single-Point Energy Calculations with the M06-2X/6-31++G(2d,p) Basis Set on M06-2X/ECP/6-31G(d) Optimized Geometries Including M06-2X/ECP/6-31G(d) Zero-Point Vibrational Energies (kJ/mol)

$1Zn^+$•→$2Zn^+$•	$3Zn^+$•→$4Zn^+$•	$1Zn^+$→$2Zn^+$	$3Zn^+$→$4Zn^+$	$5Zn^+$→$6Zn^+$	$7Zn^+$→$8Zn^+$
196	133	111	35	12	189

Scheme 6. Carbon monoxide loss from $[b_2–H + Zn]^+$ is initiated by ring-opening of the deprotonated oxazolone group. The corresponding transition state is $6Zn^+$, which is 12 kJ/mol above $1ZnB^+$, and the resultant complex containing a ketene group, $7Zn^+$, is less stable than $5Zn^+$ by 8 kJ/mol. Subsequently, $3ZnB^+$ undergoes carbon monoxide loss via transition state $8Zn^+$, forming a deprotonated a_2 fragment having negative charge on the α-carbon atom. The barrier for the carbon monoxide loss is 189 kJ/mol and the carbon monoxide loss resulted in the formation of the $[Zn/a_2–H/y'_2]^+$ complex ($9Zn^+$), in which the $[a_2–H]^-$ and y_1 were linked together via Zn^{2+} that coordinates with both His side chains, amino groups, carbonyl group and the negatively charged C_α atom. Complex $9Zn^+$ was 123 kJ/mol less stable than $1Zn^+$. The complete dissociation of $1Zn^+$• to the Zn^{2+}-adducted a_2, y'_1, carbon monoxide, and hydrogen atom requires 373 kJ/mol. The transition state barriers for the fragmentation of $[His_3–H + Zn]^+$ are summarized in Table 2.

In contrast to the fragmentation processes shown in Scheme 6, $[His_3 + Zn]^+$ containing [1H,2H]-type imidazoline group would undergo peptide bond cleavage prior to hydrogen atom release. The formation mechanism of $[b_2 + Zn]^+$ containing [1H,2H]-type imidazoline group and y'_1 fragment are shown in Supporting Information, Scheme S2. The transition state barriers for the peptide bond cleavage and subsequent proton transfer are 113 kJ/mol and 33 kJ/mol, respectively, which are similar values as shown in Table 2. In consequence, the presence of [1H,2H]-type imidazoline group has no effect on the transition state barrier for the backbone fragmentation. Notably, the radical products are not observed in ECD mass spectra of $[His_3 + Zn]^{2+}$, suggesting hydrogen atom release to occur prior to or during backbone fragmentation.

The barriers for the formation of fragments attributable to peptide bond cleavage ($[a_2–H + Zn]^+$ and $[b_2–H + Zn]^+$) are much higher than those previously reported for $[z•_2–H + Zn]^+$ and $[c'_2–H + Zn]^+$ formation. Notably, the formation of $[a_2–H + Zn]^+$ and $[b_2–H + Zn]^+$ require 286 and 373 kJ/mol, respectively, which is lower than the recombination energy of $[His_3 + Zn]^{2+}$ (522 kJ/mol). The fragment ions due to peptide bond and N–C_α bond cleavage are produced from charge-reduced products with different electronic states. Consequently, the yields of fragments due to N–C_α and peptide bond cleavage reflect the amounts of ground-state and excited-state charge-reduced products, respectively. The capture of a free electron by $[His_3 + Zn]^{2+}$ highly favors the formation of the excited-state product containing an imidazole radical, whereas the ground-state product is selectively produced by electron transfer from the fluoranthene anion to $[His_3 + Zn]^{2+}$.

Conclusion

The ECD and ETD mechanisms for Ni^{2+}-, Cu^{2+}-, and Zn^{2+}-histidine oligomer complexes were studied. Electron association to Ni^{2+}- and Cu^{2+}-histidine oligomer complexes led to reduction of the metal, and the recombination energy was redistributed throughout the complex to induce fragmentation. Comparing ECD and ETD, charge-reduced complexes with higher vibrational excitations were formed by ECD. In contrast, the Zn^{2+}-histidine oligomer complex generated a zwitterionic product, and the fragment ions obtained by ECD and ETD were different. ETD of the Zn^{2+}-polyhistidine led to aminoketyl anion radical formation followed by N–C_α bond cleavage. In contrast, ECD of the Zn^{2+}-histidine oligomer complex preferentially produced an imidazoline radical followed by hydrogen radical loss. As a result, fragment ions in the ECD mass spectra originated from the fragmentation of even-electron complexes.

Acknowledgments

The authors acknowledge support for this work by JSPS KAKENHI grant number 26505016. The computations of molecular structures were performed using the Research Center for Computational Science, Okazaki, Japan.

References

1. Zubarev, R.A., Kelleher, N.L., McLafferty, F.W.: Electron capture dissociation of multiply charged protein cations. a nonergodic process. J. Am. Chem. Soc. **120**, 3265–3266 (1998)
2. Syka, J.E., Coon, J.J., Schroeder, M.J., Shabanowitz, J., Hunt, D.F.: Peptide and protein sequence analysis by electron transfer dissociation mass spectrometry. Proc. Natl. Acad. Sci. U. S. A. **101**, 9528–9533 (2004)
3. Kelleher, N.L.: Top-down proteomics. Anal. Chem. **76**, 196A–203A (2004)
4. Coon, J.J.: Collisions or electrons? Protein sequence analysis in the 21st century. Anal. Chem. **81**, 3208–3215 (2009)
5. Zhou, H., Ning, Z., Starr, A.E., Abu-Farha, M., Figeys, D.: Advancements in top-down proteomics. Anal. Chem. **84**, 720–734 (2012)
6. Zubarev, R.A., Kruger, N.A., Fridriksson, E.K., Lewis, M.A., Horn, D.M., Carpenter, B.K., McLafferty, F.W.: Electron capture dissociation of gaseous multiply-charged proteins is favored at disulfide bonds and other sites of high hydrogen atom affinity. J. Am. Chem. Soc. **121**, 2857–2862 (1999)
7. Sawicka, A., Skurski, P., Hudgins, R.R., Simons, J.: Model calculations relevant to disulfide bond cleavage via electron capture influenced by positively charged groups. J. Phys. Chem. B **107**, 13505–13511 (2003)
8. Sobczyk, M., Anusiewicz, I., Berdys-Kochanska, J., Sawicka, A., Skurski, P., Simons, J.: Coulomb-assisted dissociative electron attachment: application to a model peptide. J. Phys. Chem. A **109**, 250–258 (2005)
9. Syrstad, E.A., Tureček, F.: Toward a general mechanism of electron capture dissociation. J. Am. Soc. Mass Spectrom. **16**, 208–224 (2005)
10. Wodrich, M.D., Zhurov, K.O., Vorobyev, A., Ben Hamidane, H., Corminboeuf, C., Tsybin, Y.O.: Heterolytic N–C_α bond cleavage in electron capture and transfer dissociation of peptide cations. J. Phys. Chem. B **116**, 10807–10815 (2012)
11. Tureček, F., Julian, R.R.: Peptide radicals and cation radicals in the gas phase. Chem. Rev. **113**, 6691–6733 (2013)
12. Asakawa, D., Yamashita, A., Kawai, S., Takeuchi, T., Wada, Y.: N–Cα bond cleavage of zinc-polyhistidine complexes in electron transfer dissociation mediated by zwitterion formation: experimental evidence and theoretical analysis of the Utah-Washington model. J. Phys. Chem. B **120**, 891–901 (2016)
13. Iavarone, A.T., Paech, K., Williams, E.R.: Effects of charge state and cationizing agent on the electron capture dissociation of a peptide. Anal. Chem. **76**, 2231–2238 (2004)
14. Fung, Y.M., Liu, H., Chan, T.W.: Electron capture dissociation of peptides metalated with alkaline-earth metal ions. J. Am. Soc. Mass Spectrom. **17**, 757–771 (2006)
15. Liu, H., Håkansson, K.: Divalent metal ion–peptide interactions probed by electron capture dissociation of trications. J. Am. Soc. Mass Spectrom. **17**, 1731–1741 (2006)

16. Flick, T.G., Donald, W.A., Williams, E.R.: Electron capture dissociation of trivalent metal ion-peptide complexes. J. Am. Soc. Mass Spectrom. **24**, 193–201 (2013)
17. Asakawa, D., Takeuchi, T., Yamashita, A., Wada, Y.: Influence of metal-peptide complexation on fragmentation and inter-fragment hydrogen migration in electron transfer dissociation. J. Am. Soc. Mass Spectrom. **25**, 1029–1039 (2014)
18. Asakawa, D., Wada, Y.: Electron transfer dissociation mass spectrometry of peptides containing free cysteine using group XII metals as a charge carrier. J. Phys. Chem. B **118**, 12318–12325 (2014)
19. Bogdanov, B., Zhao, X., Robinson, D.B., Ren, J.: Electron capture dissociation studies of the fragmentation patterns of doubly protonated and mixed protonated-sodiated peptoids. J. Am. Soc. Mass Spectrom. **25**, 1202–1216 (2014)
20. Chen, X., Fung, Y.M., Chan, W.Y., Wong, P.S., Yeung, H.S., Chan, T.W.: Transition metal ions: charge carriers that mediate the electron capture dissociation pathways of peptides. J. Am. Soc. Mass Spectrom. **22**, 2232–2245 (2011)
21. Turecek, F., Holm, A.I., Panja, S., Nielsen, S.B., Hvelplund, P.: Transition metals as electron traps. II. Structures, energetics and electron transfer dissociations of ternary Co, Ni, and Zn-peptide complexes in the gas phase. J. Mass Spectrom. **44**, 1518–1531 (2009)
22. Turecek, F., Jones, J.W., Holm, A.I., Panja, S., Nielsen, S.B., Hvelplund, P.: Transition metals as electron traps. I. Structures, energetics, electron capture, and electron-transfer-induced dissociations of ternary copper-peptide complexes in the gas phase. J. Mass Spectrom. **44**, 707–724 (2009)
23. Afonso, C., Tabet, J.C., Giorgi, G., Turecek, F.: Gas-phase doubly charged complexes of cyclic peptides with copper in +1, +2, and +3 formal oxidation states: formation, structures, and electron capture dissociation. J. Mass Spectrom. **47**, 208–220 (2012)
24. Tureček, F., Panja, S., Wyer, J.A., Ehlerding, A., Zettergren, H., Nielsen, S.B., Hvelplund, P., Bythell, B., Paizs, B.: Carboxyl-catalyzed prototropic rearrangements in histidine peptide radicals upon electron transfer: effects of peptide sequence and conformation. J. Am. Chem. Soc. **131**, 16472–16487 (2009)
25. Xia, Y., Gunawardena, H.P., Erickson, D.E., McLuckey, S.A.: Effects of cation charge-site identity and position on electron-transfer dissociation of polypeptide cations. J. Am. Chem. Soc. **29**, 12232–12243 (2007)
26. Tureček, F., Yao, C., Eva Fung, Y.M., Hayakawa, S., Hashimoto, M., Matsubara, H.: Histidine-containing radicals in the gas phase. J. Phys. Chem. B **113**, 7347–7366 (2009)
27. Nguyen, H.T., Shaffer, C.J., Tureček, F.: Probing peptide cation-radicals by near-UV photodissociation in the gas phase. Structure elucidation of histidine radical chromophores formed by electron transfer reduction. J. Phys. Chem. B **119**, 3948–3961 (2015)
28. Tureček, F., Chung, T.W., Moss, C.L., Wyer, J.A., Ehlerding, A., Holm, A.I., Zettergren, H., Nielsen, S.B., Hvelplund, P., Chamot-Rooke, J., Bythell, B., Paizs, B.: The histidine effect. Electron transfer and capture cause different dissociations and rearrangements of histidine peptide cation-radicals. J. Am. Chem. Soc. **132**, 10728–10740 (2010)
29. Frisch, M.J., Trucks, G.W., Schlegel, H.B., Scuseria, G.E., Robb, M.A., Cheeseman, J.R., Scalmani, G., Barone, V., Mennucci, B., Petersson, G.A., Nakatsuji, H., Caricato, M., Li, X., Hratchian, H.P., Izmaylov, A.F., Bloino, J., Zheng, G., Sonnenberg, J.L., Hada, M., Ehara, M., Toyota, K., Fukuda, R., Hasegawa, J., Ishida, M., Nakajima, T., Honda, Y., Kitao, O., Nakai, H., Vreven, T., Montgomery, J.A. Jr., Peralta, J.E., Ogliaro, F., Bearpark, M., Heyd, J.J., Brothers, E., Kudin, K.N., Staroverov, V.N., Keith, T., Kobayashi, R., Normand, J., Raghavachari, K., Rendell, A., Burant, J.C., Iyengar, S.S., Tomasi, J., Cossi, M., Rega, N., Millam, J.M., Klene, M., Knox, J.E., Cross, J.B., Bakken, V., Adamo, C., Jaramillo, J., Gomperts, R., Stratmann, R.E., Yazyev, O., Austin, A.J., Cammi, R., Pomelli, C., Ochterski, J.W., Martin, R.L., Morokuma, K., Zakrzewski, V.G., Voth, G.A., Salvador, P., Dannenberg, J.J., Dapprich, S., Daniels, A.D., Farkas, O., Foresman, J.B., Ortiz, J.V., Cioslowski, J., Fox, D.J.: Gaussian 09; Revision D.01. Gaussian, Inc., Wallingford (2010)
30. Zhao, Y., Truhlar, D.G.: The M06 Suite of density functionals for main group thermochemistry, thermochemical kinetics, noncovalent interactions, excited states, and transition elements: two new functionals and systematic testing of four M06-class functionals and 12 other functionals. Theor. Chem. Accounts **120**, 215–241 (2008)
31. Fukui, K.: The path of chemical reactions—the IRC approach. Acc. Chem. Res. **14**, 363–368 (1981)
32. Stratmann, R.E., Scuseria, G.E., Frisch, M.J.: An efficient implementation of time-dependent density-functional theory for the calculation of excitation energies of large molecules. J. Chem. Phys. **109**, 8218–8224 (1998)
33. Zubarev, R.A.: Reactions of polypeptide ions with electrons in the gas phase. Mass Spectrom. Rev. **22**, 57–77 (2003)
34. Bythell, B.J., Harrison, A.G.: Formation of a(1) ions directly from oxazolone b(2) ions: an energy-resolved and computational study. J. Am. Soc. Mass Spectrom. **26**, 774–781 (2015)
35. Paizs, B., Suhai, S.: Fragmentation pathways of protonated peptides. Mass Spectrom. Rev. **24**, 508–548 (2005)
36. Nelson, C.R., Abutokaikah, M.T., Harrison, A.G., Bythell, B.J.: Proton mobility in b2 ion formation and fragmentation reactions of histidine-containing peptides. J. Am. Soc. Mass Spectrom. **27**, 487–497 (2016)
37. Pepin, R., Tureček, F.: Kinetic ion thermometers for electron transfer dissociation. J. Phys. Chem. B **119**, 2818–2826 (2015)
38. Chass, G.A., Marai, C.N.J., Setiadi, D.H., Csizmadia, I.G., Harrison, A.G.: A Hartree-Fock, MP2 and DFT computational study of the structures and energies of b2 ions derived from deprotonated peptides. A comparison of method and basis set used on relative product stabilities. J. Mol. Struct. (THEOCHEM) **675**(149–162) (2004)